Significance of scattering by oceanic particles at angles around 120 degree

Xiaodong Zhang,[1,*] Emmanuel Boss,[2] and Deric J. Gray[3]

[1]*Department of Earth System Science and Policy, University of North Dakota, Grand Forks, North Dakota 58202-9011, USA*
[2]*School of Marine Science, University of Maine, Orono, Maine 04469-5706, USA*
[3]*US Naval Research Laboratory Code 7231, Washington, D.C. 20375, USA*
[*]*zhang@aero.und.edu*

Abstract: Field observations and theoretical studies have shown that shapes of the volume scattering functions (VSFs) of oceanic particles in the backward directions, i.e., VSFs normalized by the total backscattering coefficient, exhibit a surprisingly low variability at angles near 120 degree, which is also confirmed by measurements of VSFs in coastal waters around the US. To investigate what this minimum variability angle (θ*) represents, we estimated mean values of the VSFs in the backward angles using four mean value theorems: mean value for integral, weighted mean value for integral, classic mean value for differentiation and Cauchy's mean value. We also estimated the angles corresponding to the minimum values of the VSFs. We found θ* to be very close to the angles representing the classic mean values for differentiation of the VSFs. The low variability is due to the fact that the classic mean values vary little with the composition and sizes of particles.

OCIS codes: (010.0010) Atmospheric and oceanic optics; (010.4450) Oceanic optics; (010.4458) Oceanic scattering.

References and links

1. R. W. Preisendorfer, *Hydrologic Optics: Introduction* (Pacific Mar. Environ. lab/NOAA, 1976), Vol. 1, p. 218.
2. J. R. V. Zaneveld, "A theoretical derivation of the dependence of the remotely sensed reflectance of the ocean on the inherent optical properties," J. Geophys. Res. **100**(C7), 13135–113142 (1995).
3. G. L. Clarke, G. C. Ewing, and C. J. Lorenzen, "Spectra of Backscattered Light from the Sea Obtained from Aircraft as a Measure of Chlorophyll Concentration," Science **167**(3921), 1119–1121 (1970).
4. A. Morel, "Optical properties of pure water and pure sea water," in *Optical Aspects of Oceanography*, N. G. Jerlov and E. S. Nielsen, eds. (Academic Press, 1974), pp. 1–24.
5. X. Zhang and L. Hu, "Estimating scattering of pure water from density fluctuation of the refractive index," Opt. Express **17**(3), 1671–1678 (2009).
6. X. Zhang and L. Hu, "Scattering by pure seawater at high salinity," Opt. Express **17**(15), 12685–12691 (2009).
7. X. Zhang, L. Hu, and M.-X. He, "Scattering by pure seawater: Effect of salinity," Opt. Express **17**(7), 5698–5710 (2009).
8. X. Zhang, L. Hu, M. S. Twardowski, and J. M. Sullivan, "Scattering by solutions of major sea salts," Opt. Express **17**(22), 19580–19585 (2009).
9. T. J. Petzold, "Volume scattering function for selected ocean waters," SIO Ref. 72–78 (Scripps Institute of Oceanography, 1972).
10. G. Kullenberg, "Scattering of light by Sargasso Sea water," Deep-Sea Res. **15**, 423–432 (1968).
11. T. Oishi, "Significant relationship between the backward scattering coefficient of sea water and the scatterance at 120 °," Appl. Opt. **29**(31), 4658–4665 (1990).
12. M. E. Lee and M. R. Lewis, "A New Method for the Measurement of the Optical Volume Scattering Function in the Upper Ocean," J. Atmos. Ocean. Technol. **20**(4), 563–571 (2003).
13. J. M. Sullivan and M. S. Twardowski, "Angular shape of the oceanic particulate volume scattering function in the backward direction," Appl. Opt. **48**(35), 6811–6819 (2009).
14. M. Chami, E. B. Shybanov, G. A. Khomenko, M. E.-G. Lee, O. V. Martynov, and G. K. Korotaev, "Spectral variation of the volume scattering function measured over the full range of scattering angles in a coastal environment," Appl. Opt. **45**(15), 3605–3619 (2006).
15. J.-F. Berthon, E. Shybanov, M. E. G. Lee, and G. Zibordi, "Measurements and modeling of the volume scattering function in the coastal northern Adriatic Sea," Appl. Opt. **46**(22), 5189–5203 (2007).

#223973 - $15.00 USD Received 30 Sep 2014; revised 20 Nov 2014; accepted 21 Nov 2014; published 11 Dec 2014

16. A. L. Whitmire, W. S. Pegau, L. Karp-Boss, E. Boss, and T. J. Cowles, "Spectral backscattering properties of marine phytoplankton cultures," Opt. Express **18**(14), 15073–15093 (2010).
17. E. Boss and W. S. Pegau, "Relationship of light scattering at an angle in the backward direction to the backscattering coefficient," Appl. Opt. **40**(30), 5503–5507 (2001).
18. X. Zhang, D. J. Gray, Y. Huot, Y. You, and L. Bi, "Comparison of optically derived particle size distributions: scattering over the full angular range versus diffraction at near forward angles," Appl. Opt. **51**(21), 5085–5099 (2012).
19. R. A. Maffione and D. R. Dana, "Instruments and methods for measuring the backward-scattering coefficient of ocean waters," Appl. Opt. **36**(24), 6057–6067 (1997).
20. G. Dall'Olmo, T. K. Westberry, M. J. Behrenfeld, E. Boss, and W. H. Slade, "Significant contribution of large particles to optical backscattering in the open ocean," Biogeosciences **6**(6), 947–967 (2009).
21. C. F. Bohren and S. B. Singham, "Backscattering by Nonspherical Particles: A Review of Methods and Suggested New Approaches," J. Geophys. Res. **96**(D3), 5269–5277 (1991).
22. R. A. Meyer, "Light scattering from biological cells: Dependence of backscatter radiation on membrane thickness and refractive index," Appl. Opt. **18**(5), 585–588 (1979).
23. D. Stramski, E. Boss, D. Bogucki, and K. J. Voss, "The role of seawater constituents in light backscattering in the ocean," Prog. Oceanogr. **61**(1), 27–56 (2004).
24. X. Zhang, M. Twardowski, and M. Lewis, "Retrieving composition and sizes of oceanic particle subpopulations from the volume scattering function," Appl. Opt. **50**(9), 1240–1259 (2011).
25. H. Czerski, M. Twardowski, X. Zhang, and S. Vagle, "Resolving size distributions of bubbles with radii less than 30 μm with optical and acoustical methods," J. Geophys. Res. **116**, C00H11 (2011).
26. M. Twardowski, X. Zhang, S. Vagle, J. Sullivan, S. Freeman, H. Czerski, Y. You, L. Bi, and G. Kattawar, "The optical volume scattering function in a surf zone inverted to derive sediment and bubble particle subpopulations," J. Geophys. Res. **117**, C00H17 (2012).
27. X. Zhang, Y. Huot, D. J. Gray, A. Weidemann, and W. J. Rhea, "Biogeochemical origins of particles obtained from the inversion of the volume scattering function and spectral absorption in coastal waters," Biogeosciences **10**(9), 6029–6043 (2013).
28. X. Zhang, R. H. Stavn, A. U. Falster, D. Gray, and R. W. Gould, Jr., "New insight into particulate mineral and organic matter in coastal ocean waters through optical inversion," Estuar. Coast. Shelf Sci. **149**, 1–12 (2014).
29. B. Epstein, "The mathematical description of certain breakage mechanisms leading to the logarithmico-normal distribution," J. Franklin Inst. **244**(6), 471–477 (1947).
30. F. S. Lai, S. K. Friedlander, J. Pich, and G. M. Hidy, "The self-preserving particle size distribution for Brownian coagulation in the free-molecule regime," J. Colloid Interface Sci. **39**(2), 395–405 (1972).
31. J. W. Campbell and C. M. Yentsch, "Variance within homogeneous phytoplankton populations, I: Theoretical framework for interpreting histograms," Cytometry **10**(5), 587–595 (1989).
32. H. C. van de Hulst, *Light Scattering by Small Particles* (Dover Publications, Inc., 1981).
33. M. Jonasz and G. R. Fournier, *Light Scattering by Particles in Water: Theoretical and Experimental Foundations* (Academic Press, 2007), p. 704.
34. G. R. Fournier, "Backscatter corrected Fournier-Forand phase function for remote sensing and underwater imaging performance evaluation," in *Current Research on Remote Sensing, Laser Probing, and Imagery in Natural Waters,* L. M. Levin, G. D. Gilbert, V. I. Haltrin, and C. C. Trees, eds. (SPIE, 2007), pp. 66150N:66151–66157.
35. G. R. Fournier and J. L. Forand, "Analytical phase function for ocean water," SPIE Ocean Optics XII **2258**, 194–201 (1994).
36. E. Lamarre and W. K. Melville, "Air entrainment and dissipation in breaking waves," Nature **351**(6326), 469–472 (1991).
37. S. A. Thorpe and P. N. Humphries, "Bubbles and breaking waves," Nature **283**(5746), 463–465 (1980).
38. S. C. Ling and H. Pao, P., "Study of micro-bubbles in the North Sea," in *Sea Surface Sound*, B. R. Kerman, ed. (Kluwer Academic Publishers, 1988), pp. 197–210.
39. H. Medwin, "*In situ* acoustic measurements of microbubbles at sea," J. Geophys. Res. **82**(6), 971–976 (1977).
40. T. J. O'Hern, L. d'Agostino, and A. J. Acosta, "Comparison of holographic and Coulter counter measurement of cavitation nuclei in the ocean," J. Fluids Eng. **110**(2), 200–207 (1988).
41. L. Bi, P. Yang, G. W. Kattawar, and R. Kahn, "Modeling optical properties of mineral aerosol particles by using nonsymmetric hexahedra," Appl. Opt. **49**(3), 334–342 (2010).
42. E. Aas, "Refractive index of phytoplankton derived from its metabolite composition," J. Plankton Res. **18**(12), 2223–2249 (1996).
43. J. Sullivan, M. Twardowski, J. R. V. Zaneveld, and C. Moore, "Measuring optical backscattering in water," in *Light Scattering Reviews 7*, A. Kokhanovsky, ed. (Springer, 2013), pp. 189–224.
44. E. Boss, L. Taylor, S. Gilbert, K. Gundersen, N. Hawley, C. Janzen, T. Johengen, H. Purcell, C. Robertson, D. W. H. Schar, G. J. Smith, and M. N. Tamburri, "Comparison of inherent optical properties as a surrogate for particulate matter concentration in coastal waters," Limnol. Oceanogr. Methods **7**, 803–810 (2009).

1. Introduction

The volume scattering function ($\beta(\theta)$, m^{-1} sr^{-1}) describes the angular distribution of scattered light by an assemblage of particles as a function of scattering angle, θ. It is one of the key determinants of the light field in the ocean [1]. The backward portion of the VSF (i.e., $90 \leq \theta$

#223973 - $15.00 USD Received 30 Sep 2014; revised 20 Nov 2014; accepted 21 Nov 2014; published 11 Dec 2014

≤180°) is of particular importance for applications of ocean color because it largely dictates the magnitude and shape of reflected solar radiation from the ocean [2] that is amenable to remote observation, say, from a satellite [3]. The backscattering coefficient (b_b, m^{-1}) is often used to quantify the overall backward scattering and is defined as

$$b_b = 2\pi \int_{\pi/2}^{\pi} \beta(\theta) \sin\theta d\theta \quad (1)$$

Both particles and seawater contribute to the volume scattering additively. Molecular scattering by seawater has been known relatively well for several decades [4] and recent improvements [5–8] allow its prediction to within 2% of laboratory measurements. In the remaining part of the paper, VSFs or $\beta(\theta)$ refers to the volume scattering function due to particles, which can be easily estimated by subtracting the seawater contribution from the measured VSFs. Normalizing $\beta(\theta)$ with b_b or alternatively the χ factor, defined as $\chi(\theta) = \frac{b_b}{2\pi\beta(\theta)} = \frac{\int_{\pi/2}^{\pi} \beta(\theta)\sin\theta d\theta}{\beta(\theta)}$, describes the shape of $\beta(\theta)$ or $1/\beta(\theta)$ in the backward directions. In the past, because of instrumentation difficulty, field measurements of the VSFs in the ocean were scant [9, 10]. Analyzing all the field data available up to his time, Oishi [11] found χ varies the least at 120° with a mean value of 1.14 and a standard deviation of ~5%. Let θ^* denote the angle at which χ exhibits minimum variability. Recent technological advancement has allowed VSFs to be measured more frequently and extensively [12, 13], which led to a renewed interest in the behavior of the χ factor [13–17]. Sullivan and Twardowski [13] found θ^* was between 110 – 120° based on an extensive data set collected by MASCOT, a prototype instrument measuring VSFs between 10 and 170° at 10° interval. Boss and Pegau [17] analyzed data collected near the LEO-15 site off the coast of New Jersey, using another prototype instrument, VSM [12] measuring VSFs at a finer angular resolution of 0.25°, and found θ^* = 118° and χ(118°) = 1.10 ± 4%. We have measured VSFs using an improved version of VSM at three coastal waters around U.S., Monterey Bay (MT), Chesapeake Bay (CB) and Mobile Bay (MB) [18]. Combining our data with the data measured at the LEO-15 site we found that while VSFs at backward angles exhibit over 2 orders of magnitude variation (Fig. 1-(a)), the χ factor shows a minimum variability at 122° and $\chi(\theta^*)$ = 1.10 ± 1.45% (Fig. 1-(b)).

The behavior of $\chi(\theta)$ has also been simulated for spherical particles following the power-law size distribution. Under this simplified assumption, $\chi(\theta)$ were modeled for different power-law exponents and different refractive indices [11, 17, 19]. Additional modeling was also done for different cut-off sizes at the small size end of power-law function and for coated particles [20]. All of simulated $\chi(\theta)$ intersect around 112 - 120°, indicating very limited variability in this angular range.

The χ represents the form of the VSFs in the backward angles, which is very sensitive to the shape [21], composition [22], and size distributions of particles and expected to vary significantly for different aquatic environment with differing particle assemblages [23]. The existence of a consistent angle at which χ values estimated from different waters exhibit little variability is intriguing. This behavior was also found for mono-specific phytoplankton cultures [16]. To further investigate this phenomenon, we examine particles of different sizes using an optical inversion technique that we recently developed [24] with results that have been validated in different studies [18, 25–28].

#223973 - $15.00 USD Received 30 Sep 2014; revised 20 Nov 2014; accepted 21 Nov 2014; published 11 Dec 2014

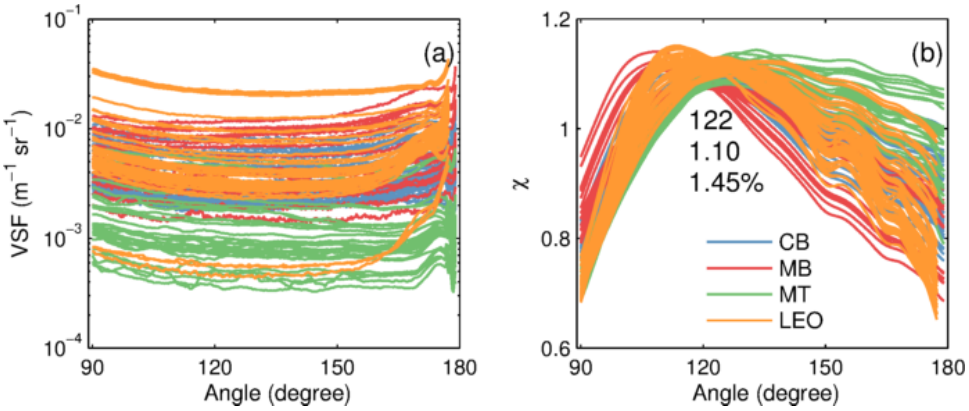

Fig. 1. (a) The backward portion of VSFs measured in Chesapeake Bay (CB), Mobile Bay (MB, Alabama), Monterey Bay (MT, California) and the LEO-15 site. (b) The χ factor estimated for the VSFs shown in (a). The three values are, respectively, the angle at which χ exhibits the minimum variability, the mean value of χ at this angle, and its coefficient of variation (std/mean).

2. Small and large particles

The technical details of the inversion method have already been reported [18, 24]. Briefly, a measured VSF is partitioned using an optimization technique into contributions by different particle species, each of which is represented by a unique combination of log-normal size distribution and composition (we use refractive index as a proxy for composition). The Log-normal function closely represents size distribution of particles resulting from natural processes of breakage [29], coagulation [30], or cell division [31]. Particles are simulated using asymmetrical hexagonal shape instead of spheres (an extreme shape having the smallest surface-area/volume). The inversion method has been tested in studies of natural bubble population [25, 26], phytoplankton and non-algal particles [27], particulate organic and inorganic matter [28] and bulk particulate size distributions [18] that are consistent with independent estimates. In this study, we will further group different particle species into two distinctive groups; small particles, representing those with sizes < 0.2 μm and large particles. There are two reasons for this approach: (1) marine particles are often operationally partitioned into dissolved (small) and particulate (large) particles via filtration; and (2) small and large particles exhibit distinctive shapes in VSFs. With this approach, we have

$$\begin{aligned} \beta(\theta) &= \beta_s(\theta) + \beta_l(\theta) \\ b_b &= b_{b,s} + b_{b,l} \end{aligned} \tag{2}$$

where subscript s and l denote small and large particles, respectively. An example of such partitioning of VSFs is shown in Fig. 2. Note that VSFs for large particles have strong forward scattering as compared to small particles.

From Eq. (2), it follows

$$\begin{aligned} \chi(\theta) &= \chi_s(\theta)\frac{\beta_s(\theta)}{\beta(\theta)} + \chi_l(\theta)\frac{\beta_l(\theta)}{\beta(\theta)} \\ &= y\chi_s(\theta) + (1-y)\chi_l(\theta) \end{aligned} \tag{3}$$

where $y \in [0,1]$. The variability of $\chi_s(\theta)$ and $\chi_l(\theta)$ was further examined for each of the four experiment sites in Fig. 3. Several features can be discerned clearly. First, χ varies but the general angular shapes are similar within each particle group. Second, the general shapes of χ differ significantly between the two particle groups. Third, the χ factor shows minimum variability at angles about 120° for both groups, even though the exact values of $\chi_s(\theta^*)$ and

#223973 - $15.00 USD Received 30 Sep 2014; revised 20 Nov 2014; accepted 21 Nov 2014; published 11 Dec 2014

$\chi_l(\theta^*)$ are different. And finally, there are insignificant differences in $\chi_s(\theta)$ or $\chi_l(\theta)$ between different experiment sites.

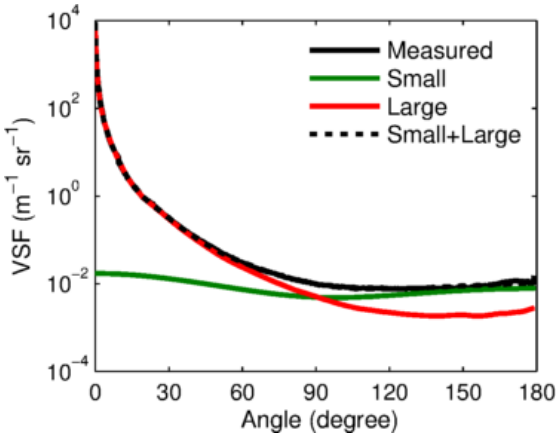

Fig. 2. A measured VSF (solid black line) is partitioned into contributions by small (green line) and large (red) particles using the inversion technique. The sum of VSFs due to small and large particles (dashed black line) matched the observed VSF nicely.

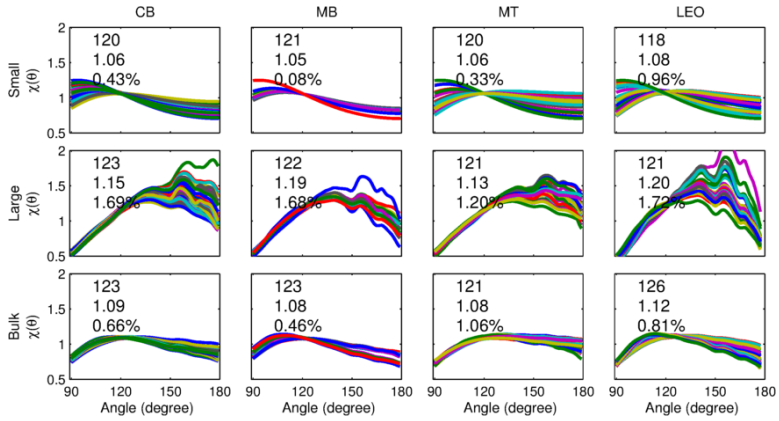

Fig. 3. The variability of χ factor estimated for two different size groups and for different experiment sites. The bulk χ is estimated using Eq. (3). The three values in each panel are, respectively, the angle at which χ exhibits the minimum variability, the mean value of χ at this angle, and its coefficient of variation (std/mean).

3. Theoretical interpretation

While both direct observation and optical inversion indicate the existence of this minimum variability angle θ^*, the question remains as to what θ^* represents? Following the weighted mean value theorem for integrals, there exists $\theta_1 \in [\pi/2, \pi]$, for which it follows from Eq. (1) that: $b_b = 2\pi\beta(\theta_1)\int_{\pi/2}^{\pi} \sin\theta d\theta = 2\pi\beta(\theta_1)$. Oishi [11] conjectured that $\theta^* \approx \theta_1$. To evaluate whether this is indeed the case, we merged $\beta(\theta)$ measured in the four field experiments into one data set and estimated θ_1 for both small and large particle groups. Figure 4 compares the values estimated for θ_1 with the minimum variability angle, θ^*. Clearly, these two angles are not the same. Actually if the two angles were the same, then $\chi(\theta^*) = 1$, differing considerably from either theoretical or experimental results that have shown $\chi(\theta^*) \approx 1.05 - 1.20$. Expanding on Oishi's approach, we estimated three other angles (θ_2, θ_3, and θ_4) $\in [\pi/2, \pi]$, based on: the

#223973 - $15.00 USD Received 30 Sep 2014; revised 20 Nov 2014; accepted 21 Nov 2014; published 11 Dec 2014

mean value theorem for integrals, $\beta(\theta_2)=\frac{2}{\pi}\int_{\pi/2}^{\pi}\beta(\theta)d\theta$; the classic mean value theorem, $\beta'(\theta_3)=\frac{2}{\pi}(\beta(\pi)-\beta(\pi/2))$; and Cauchy's mean value theorem, $\frac{\beta(\pi)\sin(\pi)-\beta(\pi/2)\sin(\pi/2)}{\sin(\pi)-\sin(\pi/2)}=\frac{(\beta(\theta_4)\sin\theta_4)'}{\cos(\theta_4)}$. The symbol ′ denotes differentiation. Note that we do not have VSF measurements at exactly 180°; the measurements were down to 177.3° in the LEO-15 experiment and down to 179° in the other three experiments. We used $\beta(177.3)$ or $\beta(179)$ directly in the above estimations. We tested by extrapolating the VSFs to 180°, with negligible differences in the estimations of these angles. Also, we estimated the minimum $\beta(\theta)$ angle (θ_5), i.e., $\beta'(\theta_5)=0$. The comparisons for these four additional angles are also shown in Fig. 4. For both small and large particle populations and for the bulk particle population, θ_3, among all the four angles, is the closest to θ^* in values and exhibits the smallest variability.

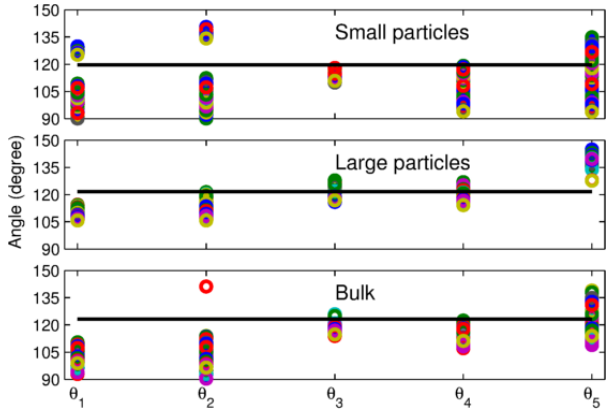

Fig. 4. Comparison of four mean value angles of θ_1, θ_2, θ_3, and θ_4 and minimum angle θ_5 (circles with various colors) with the minimum variability angle θ^* (black line) for small, large and bulk (small + large) particle populations.

Figure 4 naturally leads to a question—why are the angles (θ_3) estimated for different particle groups more similar to each other? In an attempt to answer this question, we look at two extreme cases, particles of sizes smaller than the wavelength in vacuum (λ), i.e. size $<\frac{\lambda}{2\pi m_0}$, with m_0 being the refractive index of the medium ($m_0 \approx 1.33$ for water) and particles of sizes larger than the wavelength, i.e. size $>\frac{20\lambda}{m_0}$ [32]. Assuming λ = 0.532 μm, particles smaller than the wavelength are roughly of sizes < ~0.07 μm and those larger than the wavelength of sizes > ~10 μm. For oceanic particles smaller than the wavelength, the scattering can be approximated as [32],

$$\beta(\theta)\sim 1+\frac{1-\delta}{1+\delta}\cos^2\theta \qquad (4)$$

where δ is the depolarization ratio. For oceanic particles larger than the wavelength, the scattering in the backward angles is predominately due to reflected light [33] and "*the scattering pattern caused by reflection on very large convex particles with random orientation is identical with the scattering pattern by reflection on a very large sphere of the*

#223973 - $15.00 USD Received 30 Sep 2014; revised 20 Nov 2014; accepted 21 Nov 2014; published 11 Dec 2014

same material and surface condition" [32]. Following Fournier [34], the VSF due to reflection can be approximated as:

$$\beta(\theta) \sim |r_1|^2 + |r_2|^2 + |r_1|^2 (1-|r_1|^2)^2 + |r_2|^2 (1-|r_2|^2)^2 \qquad (5)$$

where $r_1 = \dfrac{\cos\theta_i - m\cos\theta_t}{\cos\theta_i + m\cos\theta_t}$, $r_2 = \dfrac{\mathrm{m}\cos\theta_i - \cos\theta_t}{\mathrm{m}\cos\theta_i + \cos\theta_t}$, $\sin\theta_i = m\sin\theta_t$, and $\theta = \pi - 2\theta_i$. Here and hereafter, m represents the refractive index of particles relative to water. We estimated the values for the five angles of (θ_1, θ_2, θ_3, θ_4 and θ_5) from Eq. (4) for particles smaller than the wavelength and they are 125°, 135°, 110° 145° and 90°, respectively. Similarly, we estimated the values from Eq. (5) for particles much larger than the wavelength. They vary slightly with the refractive index, and range approximately 111 – 112° for θ_1, 116 – 117° for θ_2, 117 – 119° for θ_3, 120 – 122° for θ_4, and 180° for θ_5, respectively. Between the two sets of estimates, the difference for θ_3 is the smallest, varying only 7 – 9° between extremely small and large particles, whereas the differences for other angles are at least 15° or larger. Two interesting notes regarding the minimum $\beta(\theta)$ angle (θ_5): it shifts from 90° for particles smaller than the wavelength to 180° for particles larger than the wavelength and its value does not change with the refractive index for extremely large particles (geometric optics).

Next, we examine if these two extreme cases would form a bounding constraint. In nature, particles form a continuum in sizes, ranging from molecules to particulates of sizes millimeters or larger and all contribute to the volume scattering functions. The $\beta(\theta)$ by oceanic particles is often approximated using Fournier and Forand [35] phase function [see also 33], developed based on two simplified assumptions: particles follow a power law (or Junge) size distribution and have the same refractive index, with the values of the power-law exponent and index of refraction relative to water varying −5.0 – −3.5 and 1.02 – 1.20, respectively [33]. Figure 5 shows the variation of θ_3 estimated for the Fournier and Forand phase functions as a function of the power-law exponent (or Junge slope) and the refractive index of particles. Relatively, θ_3 is found to be more sensitive to the size distribution than the composition of particles. For size distributions favoring the smaller particles with a steeper slope, the values of θ_3 are close to the theoretical value of 110° estimated for particles of sizes less than the wavelength, and θ_3 approaches 120° as large particles become increasingly dominant. This indicates that the variability of θ_3 is well constrained, at least from this simplified theoretical analysis. Our result is consistent with the early finding by Boss and Pegau [17] showing that $\chi(117)$ based on Fournier and Forand phase functions have roughly the same value as $\chi(117)$ by seawater, for which $\beta(\theta)$ is the same as Eq. (4) for particles smaller than the wavelength.

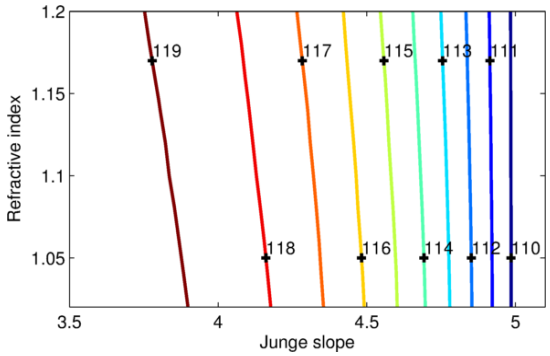

Fig. 5. Variations of θ_3 estimated for the Fournier and Forand phase functions with the exponent (or Junge slope) of the power law size distribution and the refractive index of particles.

We now examine bubbles, which are found in copious amounts in both rough [36, 37] and quiescent seas [38–40]. With m = 0.75, a (large) bubble behaves optically different from a

#223973 - $15.00 USD Received 30 Sep 2014; revised 20 Nov 2014; accepted 21 Nov 2014; published 11 Dec 2014

typical particle, whose m > 1. Since Eq. (4) does not depend on the particle type, the five angles (θ_1, θ_2, θ_3, θ_4 and θ_5 = 125°, 135°, 110°, 145° and 90°, respectively) are the same for a bubble and a particle both of sizes smaller than the wavelength. But these five angles are quite different at sizes much larger than the wavelength between a bubble and a particle; for a bubble these five angles are 108°, 112°, 110°, 114°and 180°, respectively, as compared to 111 – 112°, 116 – 117°, 117 – 119°, 120 – 122°, and 180°, respectively, for particles of different refractive indices. Interestingly, values of θ_3 for bubbles are nearly the same (= 110°) between the two extreme sizes, whereas the values for other angles differ significantly. Since the Fournier and Forand phase functions do not apply to bubble populations, we estimated $\beta(\theta)$ using Mie theory (bubbles are basically spherical) and five angles assuming the same power-law size distributions. For the exponent from −5 to −3.5, θ_3 varies from 114° to 108°, tightly around 110° which is found for both extremely small and large bubbles.

4. Discussion

We have shown that the angle θ* at which minimum variability has been observed in the backward shape of $\beta(\theta)$ represents the location of the classic mean value of $\beta(\theta)$ (we denote this angle as θ_3 in this study). While $\beta(\theta)$ in the backward angles is expected to vary strongly with the size, composition and shape of particles, the values of θ_3 are surprisingly invariant. In terms of particles sizes, we have examined variations of θ_3 in two general size fractions of dissolved and particulate (Fig. 4), in two end size members (Eqs. (4) and (5)), and in varying proportions of small and large particles. In terms of the effect of particle shape, our inversion method (Fig. 2) uses asymmetrical hexahedra to represent particles [41] and the reflective contribution to $\beta(\theta)$ was estimated using spheres. The former is almost a diametrical opposite to the latter: asymmetry vs symmetry and sharp edges vs smooth curvature. In terms of composition, the refractive indices used in the inversion and simulation cover the typical range for oceanic particles [42] and bubbles. While not exhaustive, our analyses do cover a wide range of possible representations of oceanic particles over a variety of water types. The values of θ_3 estimated over all these analyses varied within a tight range of 110 – 125°.

In remote observation of the aquatic environment (i.e., ocean color), the magnitude of the reflected signal is directly proportional to b_b, which is very difficult to measure accurately (see Eq. (1)). The existence of a minimum variability angle θ* for $\beta(\theta)$ in the backward angular range has led to practical applications, because it is possible to infer b_b relatively accurately by measuring scattering at the angle of θ* (~120°). For example, commercial sensors are available measuring scattering at fixed angles [19, 43], from which b_b are estimated.

Boss *et al.* [44] showed that scattering measured around 120° performs better as a predictor of particulate matter concentration (or total suspended solids) than measurements of side-scattering at 90° or the attenuation coefficient at coastal sites. Generally, VSFs vary strongly with the concentration, size distribution and type of particulate matter in the water [28]. However, taking measurement of VSFs around 120°, approximately representing the classic mean value of VSFs in the backward angular range that we have shown is not very sensitive to the size distribution and composition of particles, leaves the dominant sensitivity attributable to the concentration.

Even though θ_3 is most consistent with θ* and this numerical consistency remain relatively unchanged for different particle assemblages either by simulations or observations, we do not know its physical root. It remains to be investigated as to what physical connotation the classic mean value of $\beta(\theta)$ in the backward angles carries that leads to such a constrained variability?

Acknowledgments

XZ acknowledges the funding support from National Aeronautics and Space Administration (NASA) (NNX13AB20A, NNX13AN72G). EB acknowledges funding support from the Office of Naval Research (00014-13-1-0146). We thank two anonymous reviewers for their valuable comments.